Proceedings of the ASME 2010 3rd Joint US-European Fluids Engineering Summer Meeting and 8th International Conference on Nanochannels, Microchannels, and Minichannels
FEDSM-ICNMM2010
August 1-5, 2010, Montreal, Canada

FEDSM-ICNMM2010-30458

NUMERICAL INVASTIGATION ON AERODYNAMIC PERFORMANCE OF TWISTED BLADE FOR HUMAN POWERED HELICOPTER

Ryosuke HAYASHI
Department of Mechanical Engineering, Tokyo University of Science, Tokyo, Japan
j4510642@ed.kagu.tus.ac.jp

Masaya SUZUKI
Department of Mechanical Engineering,
Tokyo University of Science, Tokyo, Japan
masaya@rs.kagu.tus.ac.jp

Makoto YAMAMOTO
Department of Mechanical Engineering,
Tokyo University of Science, Tokyo, Japan
yamamoto@rs.kagu.tus.ac.jp

ABSTRACT

It is a dream for the human to freely fly in the sky by his/her own power. A human powered airplane has been developed and now we can fly for more than 100 km, while nobody has arrived at the height more than 1 m by a human powered helicopter. Therefore, the realization of a human powered helicopter will be a next dream of the human. The weight reduction is one of the most critical problems to realize a human powered helicopter. However, blades made of light materials are twisted and bent during hover. In this work, we perform three-dimensional simulation considering with fluid-structure interaction to obtain the design guidelines. The simulation is based on a weakly coupling followed as: (1) calculate the flow field, (2) calculate the deformation of blade, (3) remesh and return to phase (1). To investigate the blade performance, some cases of initial attack angle from 2 deg. to 20 deg. every 2 deg. are conducted. The results show that the optimum initial attack angle is 8 deg. and then total lift obtained by the blade is 1.36 kN. This would be sufficient for realizing a human powered helicopter.

INTRODUCTION

Flying in the sky only with human power is one of human dreams. Human powered flight is classified into two groups. One is a human powered airplane and the other is a human powered helicopter. The development of human powered airplanes began with announcement of the Kremer prize in 1959, and a human powered airplane has well-developed. So, the maximum flight speed of the current world record is 44.52 km/h by Muscalair-2 (1985), and the maximum flight distance of the current world record is 115.58 km by Daedalus88 (1988). On the other hand, a human powered helicopter has studied since announcement of the Sikorsky prize in 1980. This prize sets three criteria; the first is that a helicopter must be inside 10 × 10 m^2 area, the second is that it can fly for 1 minute, and the third is that it can reach 3 m height. In comparison, the maximum height of the current world record is 30 cm and the maximum flight duration of the current world record is 19.46 s by YURI-1, Nihon University, Japan (1994). Therefore, the records completely dissatisfy criteria for the Sikorsky prize, and so a human powered helicopter has not developed for this 30 years.

One of the most critical problems to realize a human powered helicopter is weight reduction. Greatly, the blade beam of a human powered helicopter is made out of CFRP pipe and the rib is made out of foam polystyrene. The density of CFRP pipe is about 300 times larger than that of foam polystyrene. Therefore, it is necessary for the realization of a human powered helicopter that the blade beam is a light structure. However, it causes bending and twisting to blades by aerodynamic force. Hence, the consideration of the blade bending and twisting is essential to design the blades of human powered helicopters.

In this work, we computed three-dimentional flow field around twisted blades for the realization of a human powered helicopter using computational fluid dynamics (CFD). The initial attack angle of a blade which is not deformed yet is set from 2 to 20 deg. every 2 deg. for investigating the influence of the initial attack angle on aerodynamic performance. The results show that the optimum initial attack angle is 8 deg. and then

total lift obtained by the blade is 1.36 kN. This would be sufficient for realizing a human powered helicopter.

NOMENCLATURE

C_d	drag coefficient
C_l	lift coefficient
C_p	pressure coefficient
D	drag force
G	modulus of transverse elasticity
k	turbulent kinetic energy
L	lift force
M	moment
P	static pressure
P_∞	atmospheric pressure
r	distance from aerodynamic center to blade surface
s	area of blade surface
T	torque
t	time
U_∞	inflow velocity
U_i	mean velocity
u_iu_j	fluctuating velocity
x_i	Cartesian coordinates
α	attack angle
α_0	initial attack angle
ε	turbulent dissipation rate
ν_t	eddy viscosity
θ	twisted angle
ρ	density
σ_{max}	maximum bended moment
τ	viscous stress

NUMERICAL PROCEDURE

Fluid-Structure Interaction

The problem treated in the present study is mimicked as a series of steady state during the flight. We employed a weakly coupling method followed as: (1) calculate the flow field, (2) calculate the deformation of blade, (3) remesh and return to phase (1) (see Fig. 1). These procedures are continued iteratively until the flow field and blade deformation converges sufficiently.

Flow Field

The flow field is assumed to be three-dimensional, incompressible and fully turbulent. Reynolds-averaged continuity equation and Navier-Stokes equations are solved with MAC method [1]. The governing equations are expressed as:

$$\frac{\partial U_i}{\partial x_i} = 0 \tag{1}$$

$$\frac{\partial U_i}{\partial t} + \frac{\partial U_i U_j}{\partial x_j} = -\frac{1}{\rho}\frac{\partial P}{\partial x_i} - \frac{\partial u_i u_j}{\partial x_j} \tag{2}$$

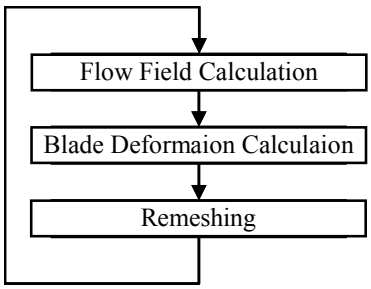

Fig. 1 Iterlation loop

where: x_i, U_i and u_i are the Cartesian coordinates, mean velocity, fluctuating velocity, respectively; t, ρ and P denote the time, density and static pressure, respectively.

In order to estimate Reynolds stresses, RNG k-ε model proposed by Yakhot-Orzack [2] is used. The transport equations of Turbulent kinetic energy and dissipation rate are expressed as:

$$\frac{\partial k}{\partial t} + \frac{\partial k U_j}{\partial x_j} = D_k + P_k - \varepsilon \tag{3}$$

$$\frac{\partial \varepsilon}{\partial t} + \frac{\partial \varepsilon U_j}{\partial x_j} = D_\varepsilon + \frac{\varepsilon}{k}\left(C_{\varepsilon 1} P_k - C_{\varepsilon 2}\varepsilon\right) \tag{4}$$

Reynolds stresses are calculated using k and ε.

$$-u_i u_j = 2\nu_t S_{ij} - \frac{2}{3}k\delta_{ij} \tag{5}$$

$$\nu_t = C_\mu \frac{k^2}{\varepsilon} \tag{6}$$

$$S_{ij} = \frac{1}{2}\left(\frac{\partial U_i}{\partial x_j} + \frac{\partial U_j}{\partial x_i}\right) \tag{7}$$

where: ν_t is the turbulence viscosity; S_{ij} is the strain rate tensor; P_k is the production term of k; D_k and D_ε are the diffusion terms of k and ε, respectively.

$$P_k = \frac{1}{2}\nu_t\left(\frac{\partial U_i}{\partial x_j} + \frac{\partial U_j}{\partial x_i}\right)^2 \tag{8}$$

$$D_k = \frac{\partial}{\partial x_j}\left(\frac{\nu_t}{\sigma_k}\frac{\partial k}{\partial x_j}\right) \tag{9}$$

$$D_\varepsilon = \frac{\partial}{\partial x_j}\left(\frac{\nu_t}{\sigma_\varepsilon}\frac{\partial \varepsilon}{\partial x_j}\right) \tag{10}$$

The model parameters are given as:

$$C_\mu = 0.085,\ C_{\varepsilon 1} = 1.42 - C_{1R},\ C_{\varepsilon 2} = 1.92$$
$$\sigma_k = 0.7179,\ \sigma_\varepsilon = 0.7179 \tag{11}$$
$$C_{1R} = \frac{\eta\left(1 - \frac{\eta}{4.38}\right)}{1 + 0.015\eta^3},\ \eta = \sqrt{2S_{ij}S_{ij}}\,\frac{k}{\varepsilon}$$

The first-order explicit method is employed for the time integration. The convection terms are discretized by Kawamura-Kuwahara third-order upwind scheme (1984). The second-order central difference is used for the other terms.

Blade Deformation Calculation

The blade consists of a spar, ribs and a skin (see Fig. 2). Since the spar almost supports the fluid force acting on the blade, the deformation of the blade is assumed to be only the twist of the spar. The spar geometry is a hollow round bar. The spar center is set on the aerodynamic center of the blade. The twisted angle by rotation of the blade is obtained from the torque generated around the blade. Thus, the twisted angle is calculated by following equations:

$$\theta = \frac{32T}{G\pi\left(d_e^4 - d_i^4\right)} \tag{12}$$

$$T = \oint r \cdot P ds \tag{13}$$

where θ is the twisted angle of the spar, T is the torque acting on the spar, d_e and d_i is respectively the external and internal diameter of the spar, G is the modulus of transverse elasticity, P is the static pressure on the blade surface, r is the distance from aerodynamic center to the blade surface and s is the area of the blade surface. Note that the aerodynamic center of the airfoil using the present study is the 25% chord.

COMPUTATIONAL CONDITIONS

Computational Domain and Grid

In this work, the designed helicopter has an double reversal revolution rotor with four blades (see Fig. 3). Only one blade is simulated because of the periodicity. The computational domain is wide enough (20 times chord length) to be free from the boundary effect. The computational domain and the computational grid are shown in Fig. 4. It should be noted that every 3 grid line is plotted in this figure The computational grid is C-type and the grid number is 301 × 61 × 31 in the computations. This grid number is selected by comparison of preliminary computations with different grid number: 241 × 51 × 31, 301 × 61 × 31, 361 × 61 × 31, 401 × 81 × 30. The grid used for present study is the most reasonable from the view point of computational costs and numerical accuracy. This grid number is obtained from the comparison between experimental

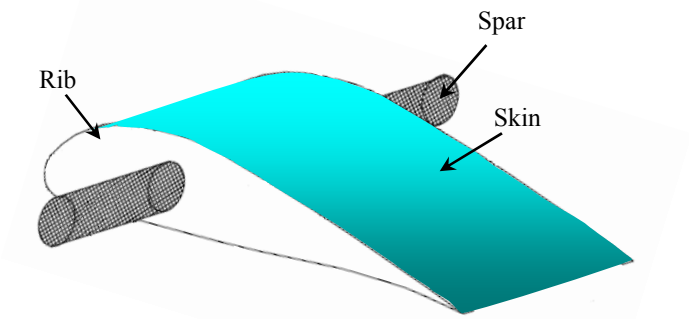

Fig. 2 Schematic of blade structure

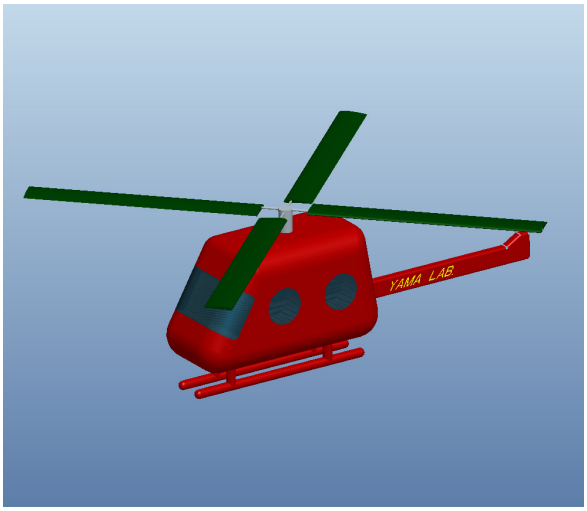

Fig.3 Helicopter with 4 blades

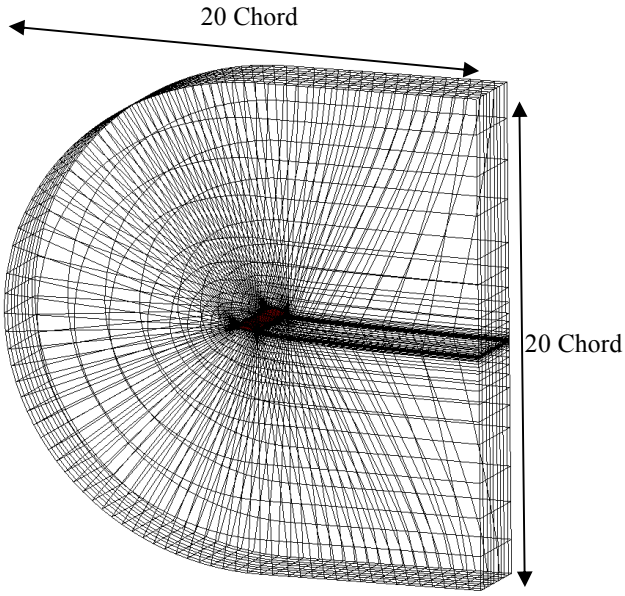

Fig. 4 Computational grid (every 3 grid point)

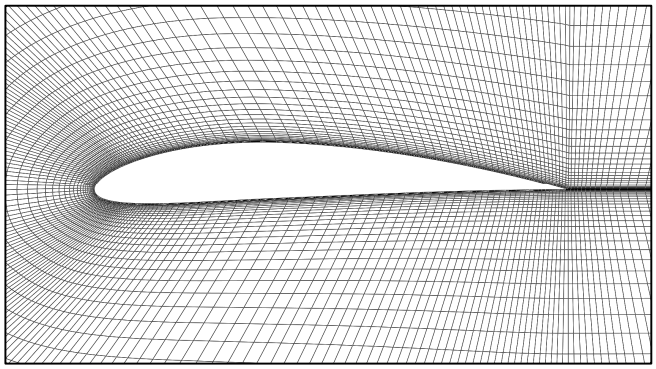

Fig. 5 Enlarged view of computational grid

data and computational data (see Table 1). A certain number of grid points are clustered near the blade surface. The enlarged view of computational grid is shown in Fig. 5.

Boundary Conditions

The following boundary conditions are imposed. At the inflow boundary, inflow speed, angle, turbulent energy and dissipation rate are fixed, and in addition pressure is extrapolated from the computational region. The rotaing speed is constant and the incidence angle is 0 deg. At the outflow, hub and tip boundaries, all variables are extrapolated from the computational region. On the blade surface, no-slip condition is used, and the general wall function for turbulent quantities is employed. It should be noted that the mean pressure in the whole computational domain is fixed.

Design Conditions of Blade

NACA4412 [5] airfoil is adopted in this study, because it has a relatively high lift to drag ratio. In Table 1, the design conditions of the blade are listed. For simplification, the blade is two-dimensionally designed, and so the blade geometry is constant for the spanwise direction. As the spar material, CFRP is adopted. As the rib material, foam polystyrene is chosen because it is very light and can be tuned to change the stiffness coefficient. The center of CFRP pipe is located on 25% of the blade chord where the aerodynamic center of NACA4412 exists [6] [7]. CFRP pipe has a circular cross section. The bend strength of CFPR pipe is 377 MPa using the volume of content rate 65% [8] [9]. A safety coefficient is assumed to be 1.2 in the present calculations. To investigate the influence of the stagger angle on aerodynamic performance, the blades are attached to the rotor shaft with the angle from 2 to 20 deg. every 2 deg. Since the free-stream angle is 0 deg., the initial attack angle is equal to the attachment angle.

RESULT AND DISCUSSION

Change of Attack Angle due to Blade Deformation

The torque acting on the blade twists the spar. The torque is calculated by integrating the static pressure over the blade surface. Since the spanwise different of the torque causes defferent attack angle for the cross section. A typical example of the bird's eye view of twisted blades is illustrated in Fig. 6. The twist angle increases from the hub to the tip. The change of twist angle at whole cross section is shown in Fig. 7. In this work, the attack angle at the hub is fixed. The closer to the tip, the larger twist angle becomes. The twist angles from the hub to the tip are about 3.5 deg. in the all cases except cases of 18 and 20 deg.

Next, the twist angles at the midspan and tip are shown in Fig. 8. It shows that the twist angle at the midspan increases as the initial attack angle is increased. In cases of 18 and 20 deg., the separation occurs at the tip and makes the pressure difference between the leading edge and trailing edge large, and so the twist angle rapidly increases over the 18 deg. case.

Figures 9 and 10 plot the pressure coefficient at the midspan and tip. The horizontal axis means the distance from the leading edge normalized by the axial chord length. The pressure coefficient is as follows:

$$c_p = \frac{P - P_\infty}{\frac{1}{2}\rho U_\infty^{\,2}} \tag{14}$$

The pressure different between the leading edge and trailing edge at the midspan increases as the initial attack angle increases. This is why the high pressure region on the pressure side becomes wide and the velocity around the suction side near the leading edge increases due to the increase of the initial attack angle. Although this tendency is almost same as the tip,

Table 1 Design conditions of blade

Airfoil		NACA4412
Rotational Speed	[rpm]	26.1
Chord Length	[m]	1.5
Span Length	[m]	5.0
Rib Material		Foam Polystylen
Spar Material		CFRP
Stiffness Coefficient of Spar	[GPa]	4.9
External Diameter of Spar	[mm]	45
Internal Diameter of Spar	[mm]	40
Total Weight of Blades	[kg]	12.3

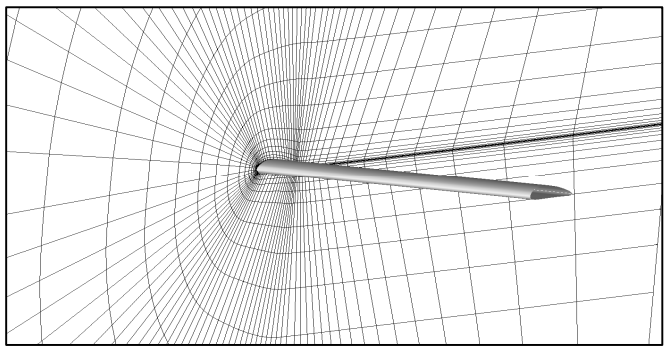

(a) Initial

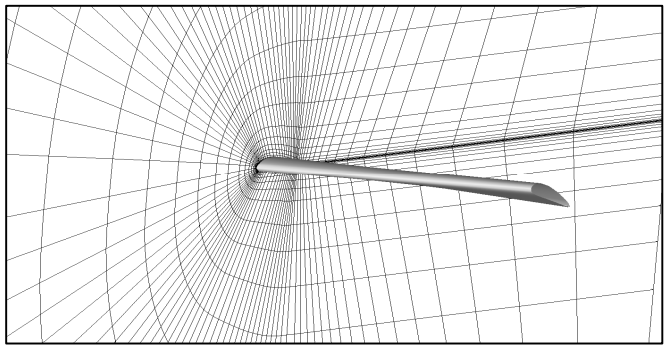

(b) Twisted

Fig. 6 Example of twisted blade

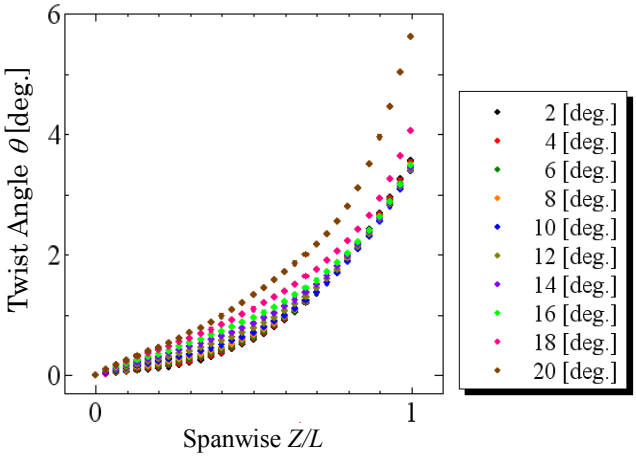

Fig. 7 Change of twist angle (cross section)

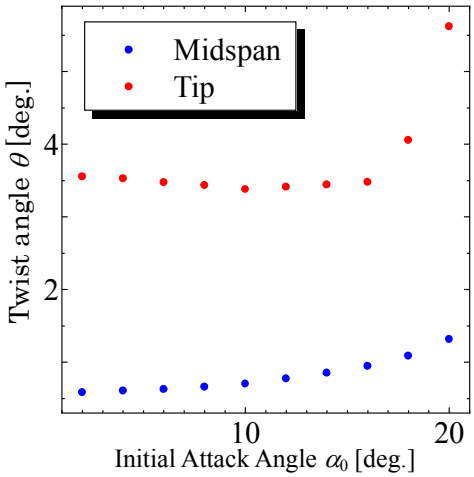

Fig.8 Change of twist angle (midspan and tip)

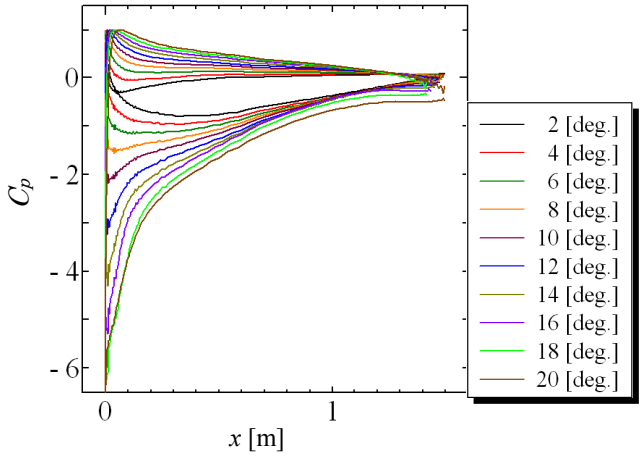

Fig. 9 Pressure coefficient at midspan

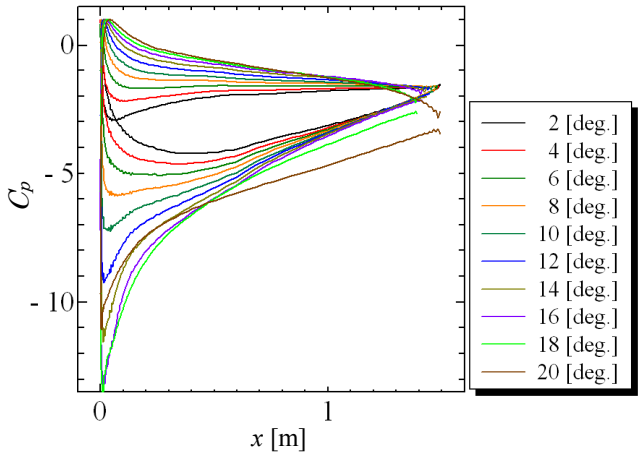

Fig. 10 Pressure coefficient at tip

the separation occurs in the cases of 18 and 20 deg. and the pressure difference between the pressure and suction surfaces decreases slightly.

Flow Field around Twisted Blade

The computational results of the flow field around the twisted blade for human powered helicopter are shown in Figs.11 to 14. All of these figures are visualized at the 90% span.

Figure11 shows velocity vectors around the twisted blade. It indicates the velocity near the leading edge is faster and the stagnation point is lower as the initial attack angle gets larger. The flow around the twisted blade is attached along the blade surface in Figs. 11(a), (b), (c) and (d), however, the separation occurs in Fig. 11(e).

Figure 12 exhibits enlarged view of velocity vectors at the 90% span near the trailing edge. In Figs. 12(a), (b), (c) and (d), the flow is smooth along the blade surface without stall as mentioned previously. However, the large separation clearly occurs in Fig. 12(e). In this work, the separation begins to occur little by little in the case of 18 deg. The stall has an undesirable effect on the blade performance. Therefore, it is very important to design the blade to prevent the separation.

Figure 13 depicts the static pressure distribution at the 90% span section. The pressure difference between the pressure surface and suction surface is larger as the initial attack angle sets larger. If initial attack angle is set to be large angle, the pressure difference increases, and so the high lift can be obtained. However, we must remember the negative effect which seriously increases the drag attached to this situation.

Figure 14 shows turbulent kinetic energy distribution at the 90% span section. Helicopter rotors have plural blades, hence, the blades are required to be designed to reduce negative influence of the wake. In Fig. 14(e), it is observed the extensive area where the turbulent kinetic energy is high. The inhomogeneous flow at the wake might degrade the blade performance of the following blade. Therefore, the blade must be designed to prevent a delay of recovery from inhomogeneous flow due to wake. In the present results, however, the highly

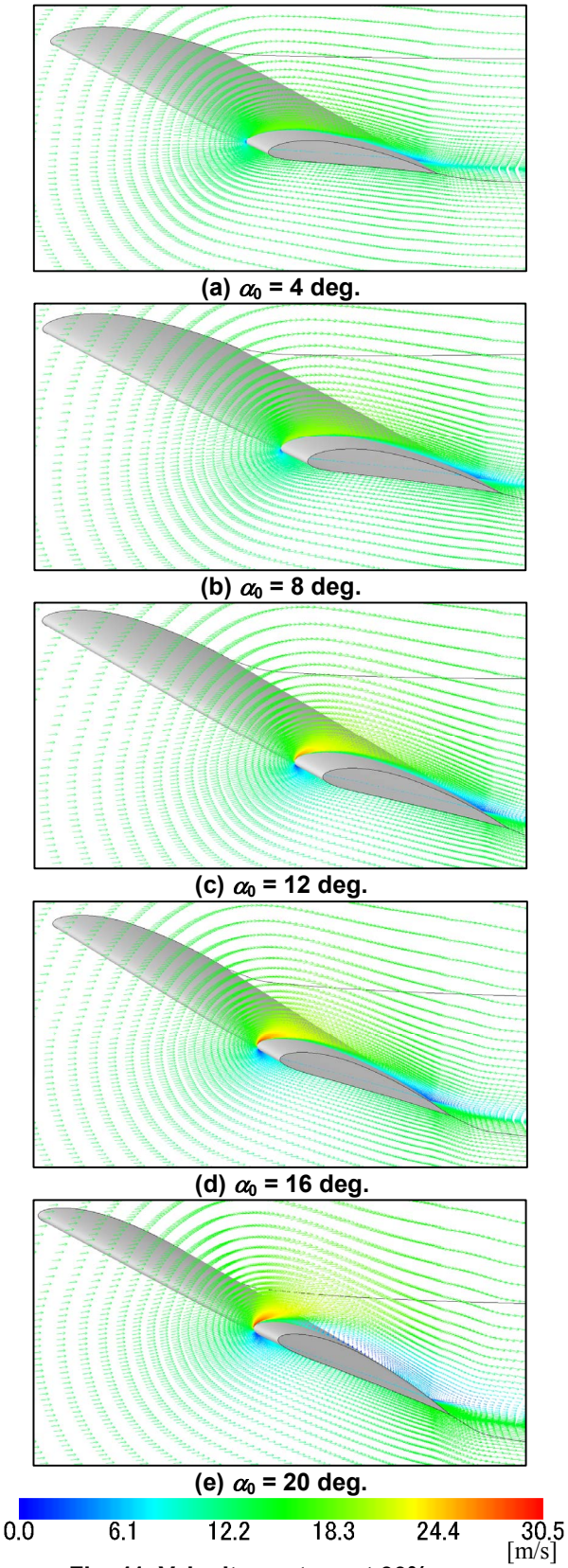

Fig. 11 Velocity vectors at 90% span

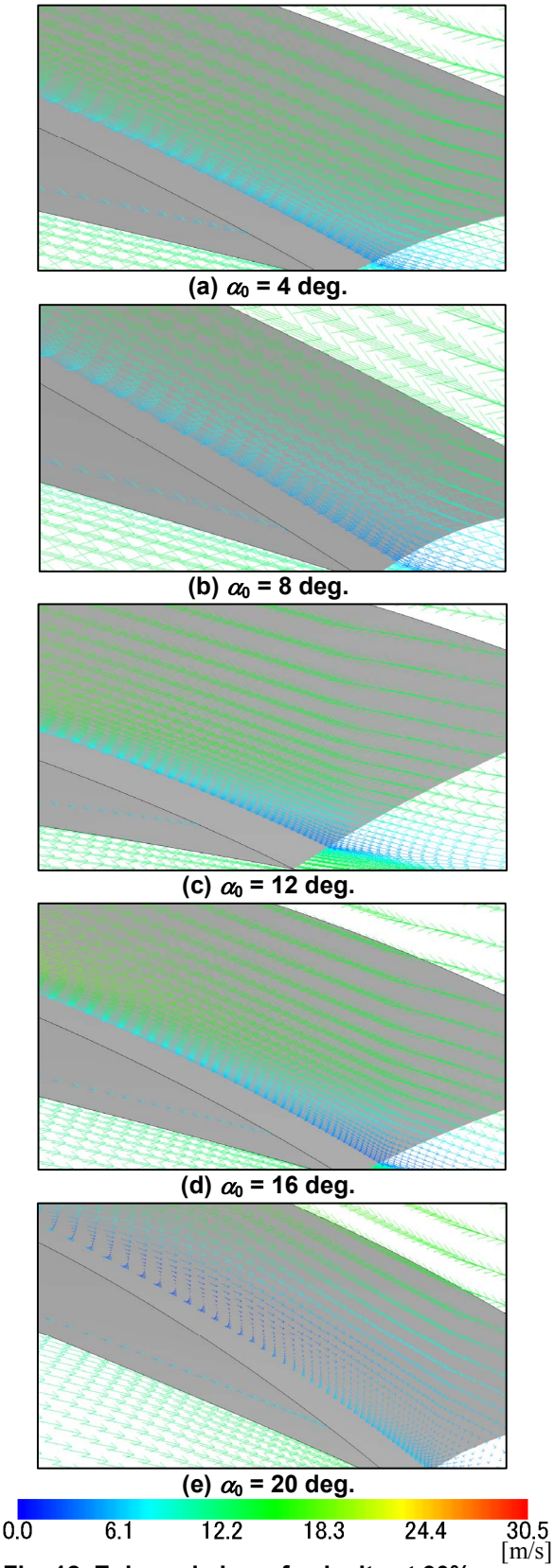

Fig. 12 Enlarged view of velocity at 90% span

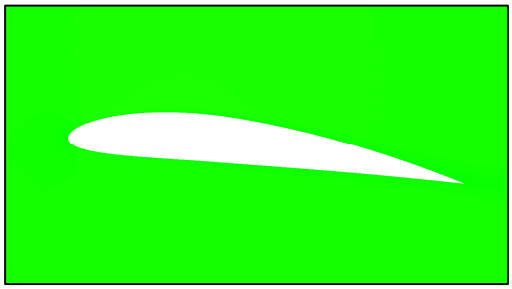

(a) α_0 = 4 deg.

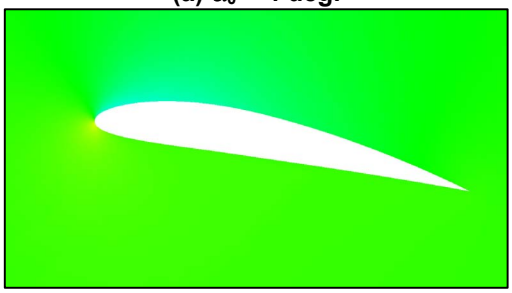

(b) α_0 = 8 deg.

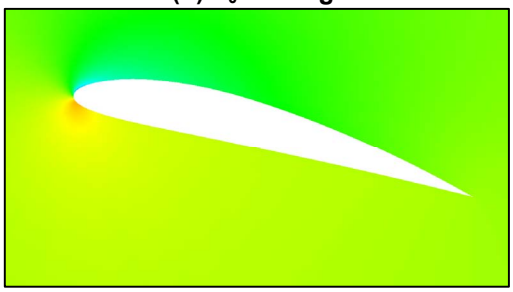

(c) α_0 = 12 deg.

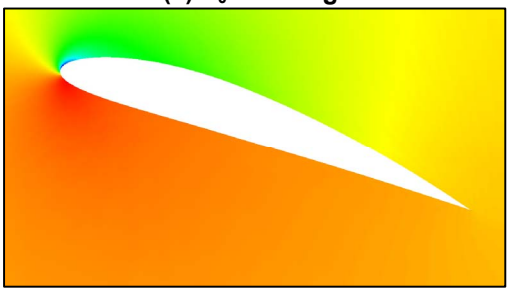

(d) α_0 = 16 deg.

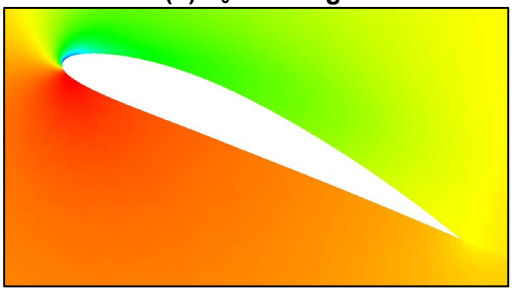

(e) α_0 = 20 deg.

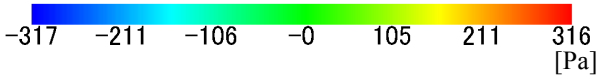

Fig. 13 Static Pressure at 90% Span

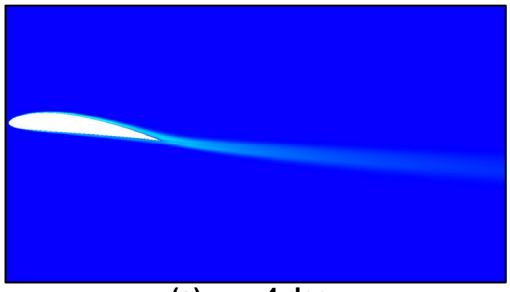

(a) α_0 = 4 deg.

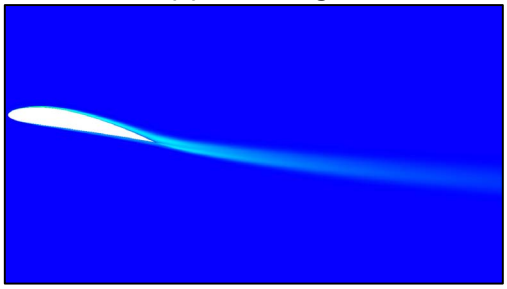

(b) α_0 = 8 deg.

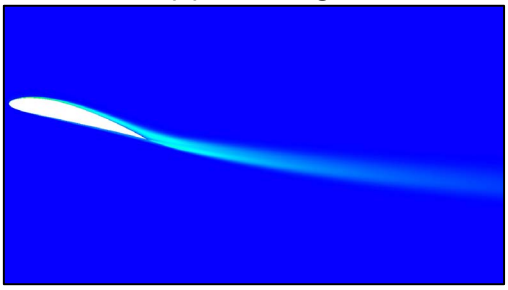

(c) α_0 = 12 deg.

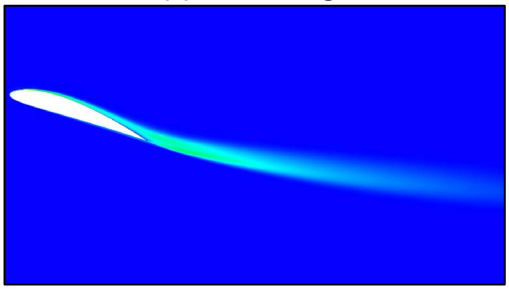

(d) α_0 = 16 deg.

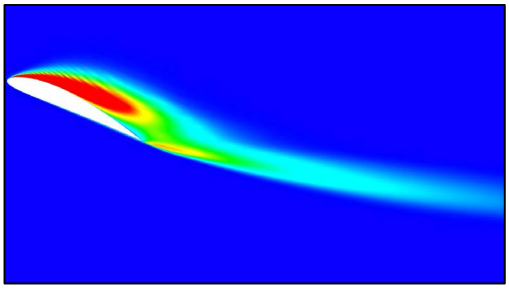

(e) α_0 = 20 deg.

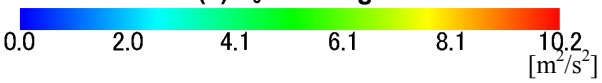

Fig. 14 Turbulent kinetic energy at 90% span

turbulent region is narrow and dissipate at the approximately 2 chord length downstream, while the wake recovery is slow as shown in Fig. 14(e). In consequence, we guess that the wake has a little influence on the following blade if the massive separation does not occur.

Aerodynamic Performance of Twisted Blade

In this work, we estimated wind performance when the blade is twisted. Integrating the static pressure and viscous stress on the blade surface, the lift and drag coefficient are calculated as follows:

$$c_l = \frac{L}{\frac{1}{2}\rho U_\infty{}^2 s} \tag{15}$$

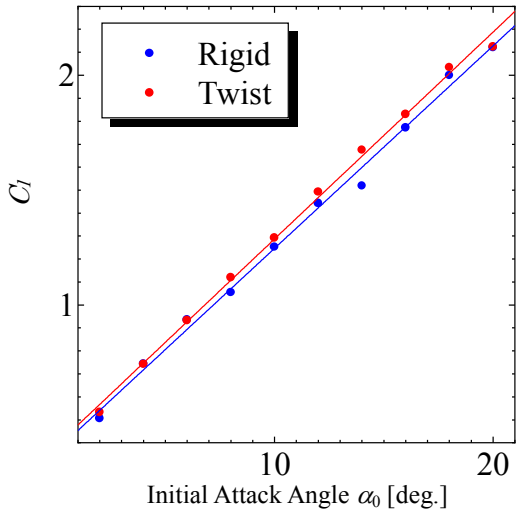

Fig. 15 Lift coefficient

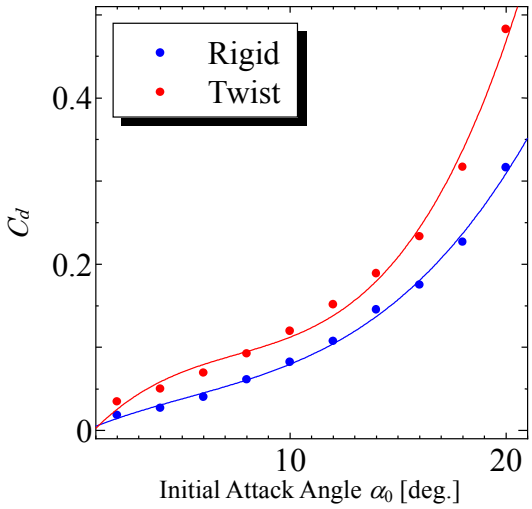

Fig. 16 Drag coefficient

$$c_d = \frac{D}{\frac{1}{2}\rho U_\infty{}^2 s} \tag{16}$$

where L and D are:

$$L = \oint \left(P\cos\alpha + \tau\sin\alpha\right) ds \tag{17}$$

$$D = \oint \left(P\sin\alpha + \tau\cos\alpha\right) ds \tag{18}$$

The lift and drag coefficients are shown in Figs.15 and 16. In addition, the lift to drag ratio is ploted in Fig. 17.

First, the results of twisted blade are compared to that of the rigid blade. The lift coefficient of the twisted blade is almost same as the results of the rigid blade. If forced to compare them, the lift coefficient of the twisted blade is a little larger. On the other hand, the drag coefficient of the twisted blade is extremely larger than that of the rigid blade; consequently, the lift to drag ratio decreases. Then, it discriminates between twisted and rigid. Therefore, it is important to take into account twist effects on the flow field in designing the blade of human powerd helicopters.

Next, the effects of the initial attack angle on the aerodynamic performance are discussed. The higher lift and drag coefficients become, the higher the initial attack angle becomes; while the lift to drag ratio decreases.

Limit of Human Power

The power generated by human is limited. The limit of human power is generally about 0.5 hp. Therefore, the blade for human powered helicopter must be designed under the load for a driver is less than 0.5 hp. The *Power* is estimated as follows:

$$Power = \oint D \times U_\infty ds \tag{19}$$

Power at different initial angles is shown in Fig. 18. It is apparent that the larger initial attack angle is, the larger the load becomes. Note that 0.5 hp is about 367.7 W. Then, the red line is the human limit in Fig. 18. Accordingly, the limit of initial

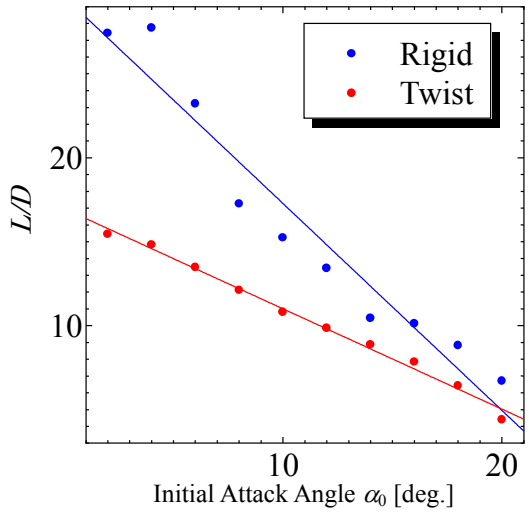

Fig. 17 Lift to drag ratio

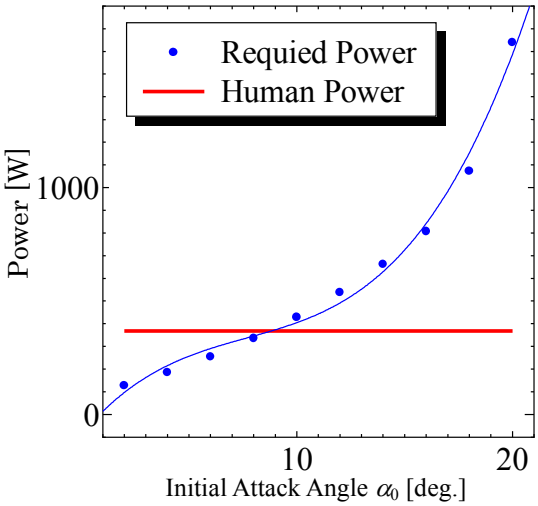

Fig. 18 Limit of human power

attack angle is 8 deg. for the present blade configuration, and this is the optimum initial angle of human powered helicopter. The blade performance of $\alpha_0 = 8$ deg. is summarized in Table 2. This is sufficient for realizing a human powered helicopter if the weight of a pilot is 60 kg and the total weight of blade and fuselage is 50 kg.

CONCLUSION

We performed three-dimentional numerical investigations based on a weakly coupling for a human powered helicopter blade. The obtained remarks are summarized as follows:

(1) The optimum initial attack angle of the blade for human powered helicopter is 8 deg.

(2) When we designed blades as outlined above, the total lift of 1.36 kN can be generated. This is sufficient for realizing a human powered helicopter.

Finally, the future work is described as follows, according to the present results. The results obtained by this work is limited to the few cases, because we designed the blade of a human powered helicopter as similar to YURI-1. There are various ways to design, e.g., airfoil, chord lengh, span length and rotational speed.

In this work, we adopted NACA4412 airfoil, because it has relatively high lift to drag ratio, lift coefficient and thin blade thickness. We didn't confirm the flow around the blade occur such large separation even the case of 20 deg. Therefore, we need to try to simulate the different airfoil which has thinner blade, and the higher lift coefficient and the higher lift to drag ratio.

The chord length was decided to be the same as YURI-1. As chord length is longer, the total lift is higher because of the increase of the blade area, although the increase of the load for drivers, the increase of the twist angle, the increase of the total weight of fuselage and so forth. If the chord and span are shorter, rotational speed can be faster while the lift decreases. Therefore, the optimum scale should be investigated.

Table 2 Blade performance

Attack Angle	α_0	[deg.]	8
Lift Force	L	[N]	340.3
Drag Force	D	[N]	28.1
Lift Coefficient	C_l		1.120
Drag Coefficient	C_d		0.092
Lift to Drag	L/D		12.1
Total Lift of 4 Blades		[kN]	1.36

We set the rotational speed 26.1 rpm such as YURI-1. The flight time of YURI-1 was only about 30 s. The human powered helicopter must flight for more 1 min. to satisfy the Sikorsky prize. Then, we need to reconsider if the driver can keep the rotational speed 26.1 rpm for more 1 min.

Furthermore, we neglected the interaction of the wake generated by the upstream blade and tip vortex in the present computations. Therefore, to obtain accurate numerical solutions, we have to carry out more sophisticated stricter simulations. For the realization of the human powered helicopter which satisfy the Sikorsky prize and more advanced criteria, we will continue further researches.

REFERENCES

[1] Harlow, F. H. and Welch, J. E., 1965, "Numerical calculation of time-dependent viscous incompressible flow of fluid with free surface", Phys. Fluids, 8, pp.2182-2189.

[2] Kim, S. W., 1991, AIAA J., 29-4, pp.547-554.

[3] Ashby, M. F. and Jones, D. R. H., 1989, "Engineering Materials", 2, Engineering Department, Cambridge University, England.

[4] National Astronomical Observatory, 2000, "Rika Nenpyo", Maruzen Co., Ltd.

[5] Abott, H. I. and Von Doenhoff, E. A., "Theory of Wing Sections", Dover Poblications, Inc.

[6] Azuma, A., 1989, "Aircraft Science and Engineering", 1, Shokabo.

[7] Azuma, A., 1989, "Aircraft Science and Engineering", 2, Shokabo.

[8] Nishikawa, T, 1998, "Flow Study of Wing selection", Nikkan Kogyo Shinbun Co.Ltd.

[9] Japanese Machine Material Society, 1997, "Machine Material Study", Kyodo Printin.

[10] Pomin. H, Wagner. S, 2002, "Aeroelastic Analysis of Helicopter Blades on Deformable Chimera Grids", AIAA Paper 2002-0951.